Laser irradiation-induced Au-ZnO nanospheres with enhanced sensitivity and stability in ethanol sensing

Hao Zhang,[a,b] Shouliang Wu, [a] Jun Liu,[a] Yunyu Cai [a] and Changhao Liang*[a,b]

a Key Laboratory of Materials Physics and Anhui Key Laboratory of Nanomaterials and Nanotechnology, Institute of Solid State Physics, Hefei Institutes of Physical Science, Chinese Academy of Sciences, Hefei 230031, China. E-mail: chliang@issp.ac.cn

b Department of Materials Science and Engineering, University of Science and Technology of China, Hefei, 230026, China.

Abstract

Incorporating noble metal nanoparticles on the surface or inner side of semiconductors to form a hybrid nanostructure is an effective route to improve the gas sensing performance of these semiconductors. In this study, we present novel Au-decorated ZnO nanospheres (Au-ZnO NSs) obtained by laser irradiation of liquids. Structural characterization indicated that the Au-ZnO NSs consisted of single crystalline ZnO NSs with few Au nanoparticles decorated on their surfaces and abundant encapsulated Au nanoparticles with relatively small sizes. Laser irradiation-induced heating–melting–evaporating processes are responsible for the formation of unique Au-ZnO NSs. Gas sensing properties of the Au-ZnO NSs, as gas sensing materials, were investigated and compared with those of pure ZnO NSs. The former showed lower working temperature, higher sensitivity, better selectivity, and good reproducibility. The response values of Au-ZnO NSs and pure ZnO NSs sensors to ethanol of 100 ppm were 252 and 75 at working temperature of 320 °C and 360 °C, respectively. The significant enhancements in gas sensing performance should be attributed to the electronic sensitization induced by the depleted layers between encapsulated Au nanoparticles and ZnO and chemical sensitization originating from the catalytic effects of Au nanoparticles decorated on the surfaces that dissociated molecular oxygen.

Introduction

Gas sensors have attracted much attention for detecting and monitoring flammable, explosive, or toxic gases as a result of the increasing concern over the effects of worsening gas pollution on health and safety. Among these gas sensors, metal oxide semiconductor (MOS) sensors are widely investigated because of their high sensitivity, low cost, and easy maintenance.[1] Seiyama et al. initially proposed the principle of gas sensing in 1962.[2] Consequently, various kinds of MOS have been explored as gas sensors. Samples of *n*-type metal oxides are ZnO, Fe_2O_3, In_2O_3, TiO_2, and WO_3. Several samples of *p*-type metal oxides are CuO, NiO, Co_3O_4, and Cr_2O_3.[3] Among candidate gas sensor nanomaterials, ZnO has been extensively investigated given its high conductivity, good stability, and biological friendliness.[4,5] However, several drawbacks, such as high operating temperature, low sensitivity, and selectivity, still limit the application of bulk ZnO as gas sensor. Numerous studies have been conducted to improve the gas sensing performance of ZnO by designing different ZnO nanostructures with large surface areas to increase active sites, such as nanocactus,[6] porous nanoflakes,[7,8] and flower-like structures.[9,10] Combining noble metal nanoparticles (NPs) (i.e., Au, Ag, or Pt) with ZnO to form hybrid nanostructures is another efficient strategy to acquire desirable sensing performance.[11–14] Two types of noble metal NP–ZnO hybrid nanostructures, namely, surface modified and encapsulated, are currently employed and generally designed to improve the sensing performance.[15–21] The gas sensing performance of sensors can be enhanced by surface modification because of the catalytic effects of the noble metal NPs in the dissociation of molecular oxygen (chemical sensitization) and electronic interaction for the formation of Schottky junctions between noble metal NPs and ZnO (electronic sensitization). However, this approach is still limited by several issues. Coagulation and chemical poisoning of noble metal NPs occur at high working temperature, resulting in the loss of catalytic activity.[1,22,23] By contrast, encapsulated noble metal NPs are more stable than that on the surface because of the protection of the surrounding

ZnO shell. Moreover, the areas of Schottky junctions in encapsulated NPs were also larger than that in surface-modified NPs because of the whole surface contact of Au with the ZnO shell. However, the catalytic effects of noble metal NPs would inevitably decline and even disappear in some cases.[24] Therefore, specific noble metal NP–ZnO hybrid nanostructures should be designed such that these hybrid nanostructures will possess the advantages of both chemical and electronic sensitization while preserving the stability of noble metal NPs under severe working conditions.

In this paper, we introduce the preparation of novel Au-decorated ZnO nanospheres (Au-ZnO NSs) with many small Au NPs encapsulated in ZnO NSs and relatively larger Au NPs decorated on the surface of ZnO NSs using laser irradiation of liquids. The Au-ZnO NS-based sensors, as sensing material, possess the combined chemical and electronic sensitization. These sensors exhibited higher sensitivity and lower working temperature towards ethanol molecules than pure ZnO NS-based sensors.

Experimental section

Chemicals and materials

Sodium hydroxide (NaOH) was purchased from the Sinopharm Chemical Reagent Co. Ltd., while Au (99.99%) and Zn (99.99%) metal plates were purchased from Beijing Goodwill Metal Technology Co. Ltd. (Beijing, China). Ultrapure water was prepared using a Milli-Q-Plus system.

Preparation of Au-ZnO NSs

First, the Au colloidal solution was obtained by ablating a piece of Au plate for 3 min in an aqueous solution of 1 mM NaOH using focused laser of 1064 nm wavelength with energy density of 80 mJ/pulse (Fig. 1). Then, the precursor of colloidal solution containing Au and ZnO NPs was synthesized by immersing the Zn plate in 18 mL of as-prepared Au colloidal solution. The plate was ablated for 10 min using focused laser of 1064 nm wavelength with an energy density of 100 mJ/pulse. Subsequently, the mixed Au and ZnO colloidal solution was further irradiated by unfocused laser with 355 nm wavelength and energy density of 40 mJ/pulse under continuous stirring for 40 min. The color of the colloidal solution changed from brown to deep purple after irradiation. Pure ZnO NSs were prepared by similar processes. Zn colloidal solution was prepared by ablating Zn plate for 10 min in an aqueous solution of 1 mM NaOH using focused laser of 1064 nm wavelength. Then, the as-prepared Zn colloidal solution was irradiated with unfocused laser of 355 nm wavelength under the same condition. The samples were washed several times with deionized water by centrifugation. Then, the products were collected and annealed in a muffle furnace at 400 ℃ for 2 h for characterization and gas sensing measurements.
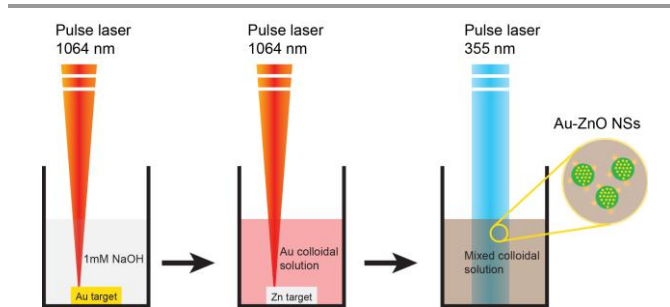

Fig. 1 Scheme of the synthesis of Au-ZnO nanospheres (NSs)

Characterization

The morphology and structure of the products were investigated using field-emission scanning electron microscopy (SU8020) and transmission electron microscopy (TEM, JEOL JEM-2010, Japan). The X-ray diffraction (XRD) patterns of all samples were recorded using a Rigaku X-ray diffractometer (G2234) with Cu–Kα radiation (λ=0.15419 nm). Photoluminescence (PL) measurements were performed with a fluorescence spectrophotometer (F-4600, Hitachi). A Keithley 6487 Source/Measure Unit (SMU) was used to record the change in current and provide a power source during testing of sensor performance.

Gas sensing Test

The gas sensors were fabricated by dispersing the Au-ZnO NSs (or pure ZnO NSs) powders in ethanol or directly coating the powders on the surface of ceramic tubes. Gas sensing measurement was conducted by injecting a certain volume of target gas (e.g., ethanol) into the chamber using a microsyringe. The target gases in the chamber were released after completion of the gas sensing measurements by flowing fresh dried air into the chamber. A constant voltage (3 V) was applied onto the sensor, and then the current was measured and acquired via SMU. The response of the sensor was calculated as follows: Response = I_g/I_a, where I_a and I_g are the electric currents of the sensor in air and target gas, respectively.
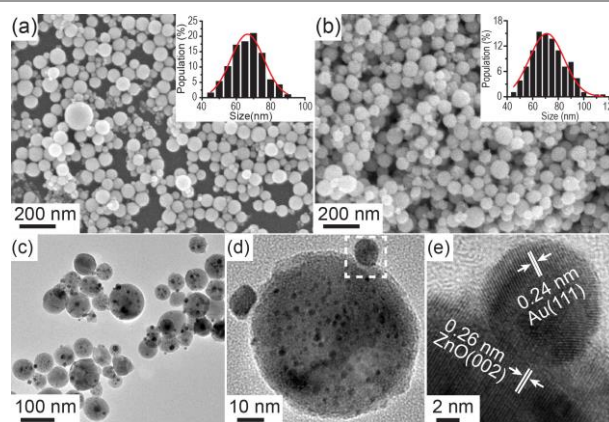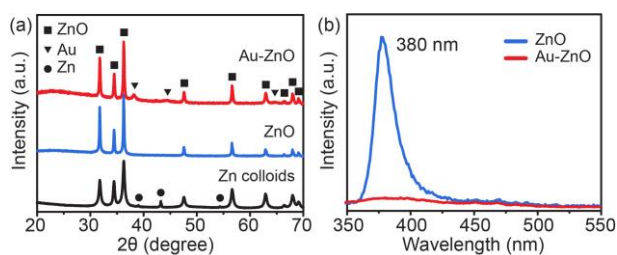
Results and Discussion

Fig. 2 Scanning electron micrographs of pure ZnO NSs (a) and Au-ZnO NSs (b); transmission electron micrographs (c) and (d) and the corresponding high-resolution transmission electron micrograph (e) of the area marked with a white dotted square in (d)

Typical scanning electron micrographs (Fig. 2a) and size distribution histogram (inset of Fig. 2a) show pure ZnO spherical morphology with an average size of 69 nm. Decoration with Au NPs resulted in spherical Au-ZnO NSs (Fig. 2b) with average size of 73 nm (inset of Fig. 2b), which is close to that of pure ZnO NSs. The transmission electron micrographs in Figs. 2c and d clearly indicated that Au-ZnO NSs were decorated with a few large Au NPs at the edge of the surfaces and encapsulated with many small Au NPs. The corresponding high-resolution transmission electron micrograph (Fig. 2e) of the area marked with white dotted square in Fig. 2d reveals the highly crystalline nature of the ZnO NSs. The clear lattice fringes with interplanar spacings of 0.26 and 0.24 nm correspond to the (002) crystalline plane of hexagonal wurtzite ZnO and the (111) crystalline plane of face-centered cubic Au, respectively. Related selected-area electron diffraction pattern (Fig. S1) also indicated the single-crystalline characteristic of ZnO NSs. Furthermore, compared with the products without annealing treatment (Fig. S2), the Au-ZnO NSs remained spherical, and no coagulation of the small Au NPs was found, thereby suggesting that the Au-ZnO NSs were very stable at high temperature.

Fig. 3 (a) X-ray diffraction patterns of as-prepared Zn colloids, pure ZnO NSs, and Au-ZnO NSs, (b) Photoluminescence spectra of pure ZnO NSs and Au-ZnO NSs excited at 300 nm

The phase structures of as-prepared Zn colloidal NPs, pure ZnO NSs, and Au-ZnO NSs were further identified by XRD characterization. The diffraction patterns in Fig. 3a indicate that all three samples contained ZnO in hexagonal structure (JCPDS card No. 01-076-0704). By contrast, XRD pattern of Zn colloids shows broadened peaks of ZnO, indicating small size of ZnO NPs, and three extra peaks with weak diffraction intensity belonging to metallic Zn. Additionally, the peaks at 38.2 °, 44.4 °, and 64.6 ° in the diffraction pattern of Au-ZnO NSs were indexed to the (111), (200), and (220) planes of cubic metallic Au (JCPDS card No. 00-004-0784), respectively. The room temperature PL spectrum (Fig. 3b) of pure ZnO NSs displays a PL emission peak at 380 nm (3.26 eV), which could be ascribed to the band edge emission of ZnO semiconductor.
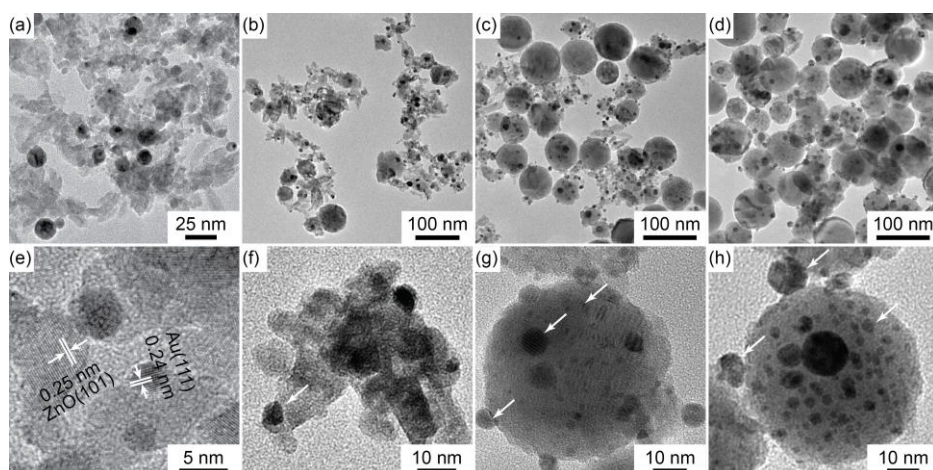
However, the emission intensity declined dramatically when the Au NPs were decorated onto ZnO. The significant decrease in the PL emission intensity of Au-ZnO NSs should be attributed to the efficient transfer of photogenerated electrons from ZnO to Au. This phenomenon suggests that significant electronic interactions occurred between Au and ZnO.

The products obtained at different irradiation times (0, 5, 20, and 40 min) were analyzed by TEM to investigate the growth mechanism involved in the synthesis of Au-ZnO NSs (Fig. 4). The product was composed of short ZnO nanorods with average diameter of 11 nm and length of 30 nm prior to laser irradiation (Fig. 4a). The high-resolution transmission electron micrograph in Fig. 4e displays the clear lattice fringes with an interplanar spacing of 0.25 and 0.24 nm, corresponding to the (101) plane of hexagonal wurtzite ZnO and the (111) plane of cubic Au, respectively. A few irregular spherical NPs with an average size of 40 nm was observed after irradiation for 5 min (Fig. 4b). The high-resolution transmission micrographs in Figs. 4f and S3 reveal the polycrystalline structure of these irregular spherical aggregates, which comprised many small rod-like ZnO and a few Au NPs, as indicated by white arrows. Increasing the irradiation time to 20 min resulted in the transformation of the irregular aggregates to NSs with average size of 65 nm (Fig. 4c), which had already exhibited the Au-ZnO hybrid nanostructures (Fig. 4g). Further increase in irradiation time to 40 min resulted in the complete consumption of rod-like ZnO nanocrystallines (Fig. 4d), instead of the formation of ZnO NSs (Fig. 4h). However, no obvious increase in the size of ZnO NSs was found compared with that of the product obtained at 20 min. This result suggests that the size of ZnO NSs reached the maximum value under the certain input laser fluence of 40 mJ/pulse. This finding could be reasonably explained by Equation (1), which quantitatively defines the maximum size of particle at certain fluence.[25,26]

$$Q_{abs} = J\sigma^{\lambda}_{abs}\left(d_p\right) = \rho_p\left(\frac{\pi d_p^3}{6}\right)\left\{C_p^s\left(T_m - T_0\right) + \Delta H_m + C_p^l\left(T_b - T_0\right) + \Delta H_b\right\}, \quad (1)$$

where J is the laser fluence, and σ^{λ}_{abs} is the absorption cross-section. Thus, the required laser fluence $J*$ that will heat a particle with diameter of d_P from room temperature (T_0) to the melting temperature (T_m) and to boiling temperature (T_b) could be determined. The density ρ_p, heat capacities C_p^s for solids and C_p^l for liquids, melting heat ΔH_m, and boiling heat ΔH_b are physical and thermodynamic constants adopted from Perry.[27]
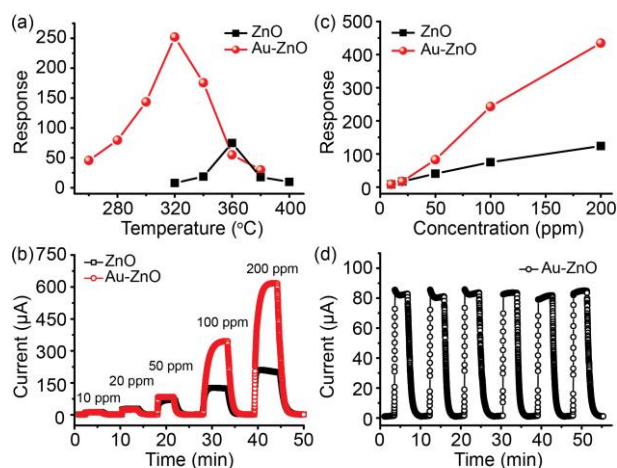
Fig. 4 Transmission electron micrographs of the products at different irradiation times in a typical growth process of Au-ZnO NSs: 0 (a, e), 5 (b, f), 20 (c, g), and 40 min (d, h). The dark dots marked by white arrows in (f–h) are Au NPs.
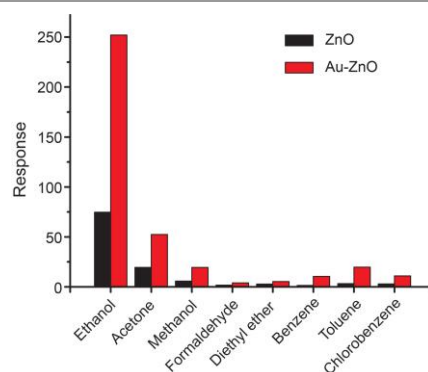
The physical heating–melting–evaporating mechanism was considered to be responsible for the formation of the Au-ZnO NSs, similar to the report of Wang et al.[26]. ZnO NPs dispersed in liquids were melted under appropriate input laser fluence. Neighboring melted NPs fused together and then remelted into larger NPs because of Brownian movement. A rapid cooling process caused by surrounding liquids occurred after pulsed laser heating (within 7 ns), leading to the formation of ZnO NSs. Some Au NPs were also melted and encapsulated inside ZnO NSs during the melting and remelting processes, whereas others were decorated on the surface of ZnO NSs.

Fig. 5 (a) Responses versus operating temperature of pure ZnO NS-based and Au-ZnO NS-based sensors to 100 ppm of ethanol. Dynamic ethanol response–recovery transients (b) and responses versus ethanol concentrations plot (c) of pure ZnO NS-based and Au-ZnO NS-based sensors at 360 ℃ and 320 ℃, respectively. (d) Cyclic dynamic response–recovery transient of Au-ZnO NSs to 50 ppm of ethanol at 320 ℃

The synergetic effects of Au NPs on gas sensing performance of ZnO were explored by performing gas sensor experiments using pure ZnO NSs and Au-ZnO NSs. Response properties of MOS are highly dependent on its operating temperature. The response of pure ZnO NSs under increasing operating temperature, reached a maximum value of 75 at 360 ℃, but the optimum operating temperature of Au-ZnO NSs was 320 ℃, which was lower than that of pure ZnO NSs (Fig. 5a). The corresponding response value was 3.4 times higher than that of pure ZnO NSs. Figure 5b shows the real-time responses of Au-ZnO NS-based or pure ZnO NS-based sensor toward different concentrations (10–200 ppm) of ethanol at 320 ℃ and 360 ℃, respectively. We clearly found that the response values of both sensors were almost the same at low concentration ($\leq$ 20 ppm) of ethanol. However, the response of Au-ZnO NS-based sensor increased rapidly and exhibited 2–4 times more than that of pure ZnO NS-based sensor when the concentration of ethanol exceeded 20 ppm. The plots of the response value versus concentration of ethanol (Fig. 5c) of the pure ZnO NS-based or Au-ZnO NS-based sensor revealed that the responses of both sensors presented approximate linear correlation with the concentrations of ethanol. The stability of the gas sensor was also considered as an important parameter. Figure 5d shows that the response of the Au-ZnO NS-based sensor did not decline and remained constant after six cycled measurements, indicating the excellent stability of the Au-ZnO NS-based gas sensor.
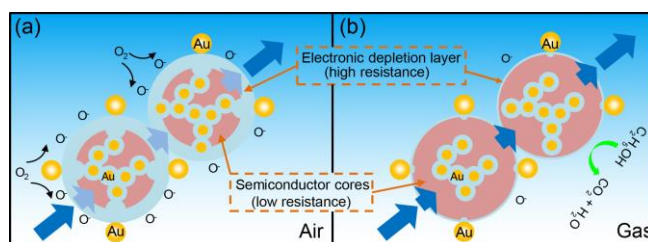
Fig. 6 Selectivity of pure ZnO NS-based (black bar) and Au-ZnO NS-based (red bar) sensors on successive exposure to 100 ppm of various gases at 360 ℃ and 320 ℃

Selectivity of gas sensor materials is highly significant in practical application. The selectivity of the pure ZnO NS-based or Au-ZnO NS-based sensor toward ethanol was evaluated by testing the sensors against various toxic gases, namely, methanol, formaldehyde, acetone, diethyl ether, benzene, toluene, and chlorobenzene. The responses of both sensors towards 100 ppm of different gases at 360 ℃ and 320 ℃ are shown in Fig. 6. The Au-ZnO NS-based sensor exhibited enhanced responses compared with the pure ZnO NS-based sensor for all gases. Both sensors show good selectivity to ethanol. The Au-ZnO NS-based sensor showed diverse responses to different gases, as follows: methanol, 19.5; formaldehyde, 4; acetone, 52.5; diethyl ether, 5.3; benzene, 10.4; toluene, 19.6; and chlorobenzene, 10.9. Remarkably, the highest response value of 252 was obtained for ethanol, indicating that Au-ZnO NSs has good selectivity to ethanol. Different morphologies with various exposed crystal planes were believed to influence gas sensing and photocatalytic behavior of metal oxides because of the diverse chemisorption abilities of the different exposed faces.[28] The morphology of ZnO could affect the selectivity of the pure ZnO-based sensor. Hamedani et al. investigated the responses of ZnO with three different morphologies (NP, nanorod, and flower-like) to CO, ethanol and methane. The NP sensor had good selectivity to ethanol.[29] Therefore, improved selectivity to ethanol of the Au-ZnO NS-based sensor could be attributed to the spherical morphology of ZnO and decorated Au NPs.

Thus, we propose the possible gas sensing mechanism of our Au-ZnO NS-based sensor by considering the electronic sensitization and chemical catalytic effects (Fig. 7). For pure ZnO, the oxygen in air could adsorb on its surface and form oxygen anions by capturing the electrons from its conduction band. This process would lead to high air resistance of ZnO sensor because of the formation of depletion layer on ZnO surface.[30,31] However, the presence of Au NPs in Au-ZnO NSs would change the energy band structure of ZnO as a result of the formation of Schottky barriers. The work function of Au metal (5.1 eV) was larger than that of ZnO (4.65 eV). Thus, the conduction band electrons of ZnO would transfer into Au NPs to form depletion layers between the ZnO shell and Au NPs. For Au-ZnO NSs prepared in our experiments, Au NPs were not only decorated on the surface of ZnO, but also encapsulated inside. Au NPs under surface decoration could increase the width of depletion layer in ZnO, which was caused by oxygen absorption. By contrast, numerous smaller Au NPs would bring numerous depletion layers around them in ZnO during encapsulation. Fig. 7a illustrates that these depletion layers might connect with each other and would evidently increase the air resistance of Au-ZnO NS-based sensor. This result agreed well with the experiment results in which the air resistance of Au-ZnO NS-based sensor (2.1 MΩ) was larger than that of pure ZnO NS-based sensor (1.7 MΩ). This characteristic implies that Au-ZnO NSs could display better sensitivity than pure ZnO NSs, which is consistent with

the aforementioned results of sensing performance. In addition to electronic sensitization, Au NPs are considered as a good catalyst to dissociate molecular oxygen because of its spillover effect.[32-34] Therefore, more molecular oxygen could be absorbed on the surface of ZnO after the decoration of Au NPs on the surface. The chemisorbed oxygen anions could react with ethanol molecules to release electrons back to the conduction band of ZnO when ZnO is exposed to reducing gas, such as ethanol (Fig. 7b). This process will lead to the decrease in the resistance of ZnO sensor. The higher the amount of chemisorbed oxygen anions, the larger would be the decrease in resistance. Thus, compared with pure ZnO NS-based sensor, the improved sensitivity of Au-ZnO NS-based sensor towards ethanol could be attributed to both electronic and chemical sensitization.

Fig. 7 Scheme of gas sensing mechanism of Au-ZnO NS-based sensor. (a) Exposure of Au-ZnO NS-based sensor to air resulted in the chemisorption of oxygen molecules onto surface of ZnO through trapping electrons. These processes could be catalyzed by Au NPs. Thus, an electronic depletion layer (represented by light blue region) was formed at the ZnO–air interface. In addition to that on the surface, the depletion layers also formed inside of ZnO because of the formation of Schottky junctions between Au and ZnO. The depletion layers both on the surface and inside may connect with each other and make the low-resistance cores discrete. Therefore, the sensor presents high resistance in air, which leads to a small current flow. (b) The width of the surface depletion layer decreases after injection of ethanol gas, which can react with absorbed oxygen species. Then, the surface depletion layers disconnect with the inside ones, and the discrete low-resistance cores become continuous. Consequently, resistance of Au-ZnO NS-based sensor decreases dramatically, which leads to a large current flow.

Conclusion

We presented the preparation of novel Au-ZnO NSs with many small Au NPs encapsulated in ZnO NSs and relatively larger Au NPs decorated on the surface of ZnO NSs using a laser irradiation of liquid approach. The Au-ZnO NSs showed perfect structural stability against annealing at 400 ℃ for 2 h. The heating–melting–evaporating mechanism was responsible for the disappearance of ZnO nanorods and formation of Au-ZnO NSs. The Au-ZnO NS-based sensor benefited from the structural stability as a gas sensing material. Thus, this sensor displayed good reproducibility, with unchanged response value during six cycled measurements. Additionally, Au-ZnO NS-based sensor showed excellent sensing performance toward ethanol, such as improved sensitivity and selectivity and reduced working temperature after the decoration of Au NPs onto the ZnO NSs. This improved sensing performance could be attributed to the catalytic effects of the surface-decorated Au NPs and the formation of depletion layers induced by the encapsulated Au NPs. Thus, such stable and hybrid nanostructure Au-ZnO NSs could be candidates for gas sensing materials.

Acknowledgement

Notes and references

1   P. Rai, S. M. Majhi, Y. T. Yu and J. H. Lee, *RSC Adv.*, 2015, **5**, 76229-76248.
2   T. Seiyama, A. Kato, K. Fujiishi and M. Nagatani, *Anal. Chem.*, 1962, **34**, 1502-1503.
3   H. J. Kim and J. H. Lee, *Sens. Actuators B,* 2014, **192**, 607-627.
4   Z. Q. Zheng, J. D. Yao, B. Wang and G. W. Yang, *Scientific reports*, 2015, **5**.
5   Y. Y. Zhao, X. Lai, P. Deng, Y. X. Nie, Y. Zhang, L. L. Xing and X. Y. Xue, *Nanotechnology*, 2014, **25**, 115502.
6   S. R. Ryu, S. G. Ram, H. D. Cho, D. J. Lee, T. W. Kang and Y. Woo, *Nanoscale*, 2015, **7**, 11115-11122.
7   M. Chen, Z. H. Wang, D. M. Han, F. B. Gu and G. S. Guo, *J. Phys. Chem. C,* 2011, **115**, 12763-12773.
8   F. L. Meng, N. N. Hou, Z. Jin, B. Sun, Z. Guo, L. T. Kong, X. H. Xiao, H. Wu, M. Q. Li and J. H. Liu, *Sens. Actuators B*, 2015, **209**, 975-982.
9   H. J. Zhang, R. F. Wu, Z. W. Chen, G. Liu, Z. N. Zhang and Z. Jiao, *CrystEngComm*, 2012, **14**, 1775-1782.
10 F. L. Meng, N. N. Hou, Z. Jin, B. Sun, W. Q. Li, X. H. Xiao, C. Wang, M. Q. Li and J. H. Liu, *Sens. Actuators B*, 2015, **219**, 209-217.
11 W. W. Xia, C. Mei, X. H. Zeng, G. K. Fan, J. F. Lu, X. D. Meng and X. S. Shen, *ACS Appl. Mater. Interfaces*, 2015, **7**, 11824-11832.
12 Q. Xiang, G. F. Meng, Y. Zhang, J. Q. Xu, P. C. Xu, Q. Y. Pan and W. J. Yu, *Sens. Actuators B*, 2010, **143,** 635-640.
13 N. Tamaekong, C. Liewhiran, A. Wisitsoraat and S. Phanichphant, *Sens. Actuators B*, 2011, **152,** 155-161.
14 N. P. Herring, K. AbouZeid, M. B. Mohamed, J. Pinsk and M. S. El-Shall, *Langmuir*, 2011, **27**, 15146–15154.
15 X. H. Liu, J. Zhang, L. W. Wang, T. L. Yang, X. Z. Guo, S. H. Wu and S. R. Wang, *J. Mater. Chem.*, 2011, **21**, 349-356.
16 J. Zhang, X. H. Liu, S. H. Wu, B. Q. Cao and S. H. Zheng, *Sens. Actuators B*, 2012, **169**, 61-66.
17 J. Guo, J. Zhang, M. Zhu, D. X. Ju, H. Y. Xu and B. Q. Cao, *Sens. Actuators B*, 2014, **199**, 339-345.
18 L. L. Wang, Z. Lou, T. Fei and T. Zhang, *J. Mater. Chem.*, 2012, **22**, 4767-4771.
19 X. W. Li, X. Zhou, H. Guo, C. Wang, J. Y. Liu, P. Sun, F. M. Liu and G. Y. Lu, *ACS Appl. Mater. Interfaces*, 2014, **6**, 18661-18667.
20 L. H. Zu, Y. Qin and J. H. Yang, *J. Mater. Chem. A*, 2015, **3,** 10209-10218.
21 S. M. Majhi, P. Rai and Y. T. Yu, *ACS Appl. Mater. Interfaces*, 2015, **7,** 9462-9468.
22 P. M. Arnal, M. Comotti and F. Schüth, *Angew. Chem. Int. Ed.*, 2006, **45**, 8224-8227.
23 J. Li and H. C. Zeng, *Angew. Chem.*, 2005, **117,** 4416-4419.
24 Y. K. Lin, Y.J. Chiang and Y. J. Hsu, *Sens. Actuators B*, 2014, **204**, 190-196.
25 A. Pyatenko, M. Yamaguchi and M. Suzuki, *J. Phys. Chem. C*, 2007, **111,** 7910-7917.
26 H. Q. Wang, A. Pyatenko, K. Kawaguchi, X. Y. Li, Z. Swiatkowska‒Warkocka and N. Koshizaki, *Angew. Chem. Int. Ed*, 2010, **49**, 6361-6364.
27 D. W. Green, R. H. Perry, *Perry's Chemical Engineers' Handbook*, McGraw-Hill, New York, 1999.
28 X. G. Han, H. Z. He, Q. Kuang, X. Zhou, X. H. Zhang, T. Xu, Z. X. Xia and L. S. Zheng, *J. Phys. Chem. C*, 2009, **113,** 584–589.
29 N. F. Hamedani, A. R. Mahjoub, A. A. Khodadadi and Y. Mortazavi, *Sens. Actuators B*, 2011, **156**, 737–742.
30 R. K. Joshi, Q. Hu, F. Alvi, N. Joshi and A. Kumar, *J. Phys. Chem. C*, 2009, **113**, 16199-16202.
31 V. Postica, I. Holken, V. Schneider, V. Kaidas, O. Polonskyi, V. Cretu, I. Tiginyanu, F. Faupel, R. Adelung and O. Lupan, *Mater. Sci. Semicond. Process.*, 2016, **49**, 20-33.
32 M. Hübner, D. Koziej, J. D. Grunwaldt, U. Weimar and N. Barsan, *Phys. Chem. Chem. Phys.*, 2012, **14**, 13249-13254.
33 Q. Xiang, G. F. Meng, H. B. Zhao, Y. Zhang, H. Li, W.J. Ma and J. Q. Xu, *J. Phys. Chem. C*, 2010, **114,** 2049-2055.
34 L. L. Wang, H. M. Dou, Z. Lou and T. Zhang, *Nanoscale*, 2013, **5,** 2686-2691.